Observation of D+D Fusion in Electromagnetically Self-Contained, Long-Lifetime Plasmoids

Dominik Kuryga Paulina Nadia Weremczuk

***Abstract* – We report the generation of self-contained, long-lived plasmoids in a low pressure coaxial diode of novel concept, driven by a ~5ns up to 1MV pulse, generating neutron bursts consistent with D+D fusion in discharges in deuterium. Neutrons were detected using a silver activation based detector. A correlation was observed between lifetime and neutron yield. Average neutron yields reached approximately 5–7x10^{5} neutrons per shot, with peak values up to 1,4x10^{6} neutrons/shot. Microwave emission measurements were done showing long decaying radiation. The demonstrated detectable nuclear fusion in this novel device opens new perspectives for compact neutron sources and alternative fusion concepts based on self-confined plasmoids.**

Keywords: plasmoid, ball lightning, inertial electrostatic confinement, D-D fusion, pulsed power, silver activation, virtual cathode

Introduction

Since the discovery in the 1930s that fusion powers the Sun, researchers have been working on devices capable of sustaining controlled fusion reactions. The first patent for a fusion reactor concept was filed already in 1951 [1]. Over the next decades fusion research has made substantial progress, both in theory and in experimental techniques, although practical energy production still remains a major challenge.

Growing global energy demand and the need to move away from fossil fuels have increased interest in nuclear fusion as a possible long-term solution. If successful, fusion could provide a stable source of carbon-free energy, free from the stability problems of wind and solar power. The best studied approaches today are tokamaks and inertial confinement fusion. Both require very large facilities and enormous resources. Because of that, alternative concepts are also being investigated - either as potential future power sources or as compact, table-top neutron generators for research and industrial use [2].

One well-known example of a small-scale device is the Inertial Electrostatic Confinement (IEC) fusor, particularly the Farnsworth-Hirsch design. In this device, ions are accelerated by an electric field between two concentric grids and can fuse in the central region. Another variant is the Polywell [3], which tries to solve the problem of ion losses on the solid grids by using a cloud of magnetically confined electrons as a virtual cathode.

Another important pulsed device is the Dense Plasma Focus (DPF) [4,5]. It belongs to the family of pinch devices and is known for its scalability. It can be operated with capacitor energies ranging from about 100 mJ up to several MJ. Because the device presented in this work is also pulsed and operates in the range of tens to hundreds of joules, the DPF provides a useful point of comparison.

A different class of compact toroidal plasmas includes Field-Reversed Configurations (FRC) and spheromaks. In these systems the plasma forms a self-organized torus and typical plasmoid lifetimes are in the range of microseconds to a few milliseconds [6].

In this work we describe a pulsed-power device that produces self-contained plasmoids with unusually long lifetimes. The plasmoid is generated by a high-voltage, high-current nanosecond pulse that excites a stable, oscillatory electromagnetic structure made of high-energy electrons. This structure acts as a virtual cathode confining energetic ions. The observed plasmoids reach lifetimes of dozens of milliseconds. The approach is scalable and, due to the absence of physical grids and nearly force-free conditions inside the plasmoid, may reduce some of the energy losses typical for fusors and Polywell devices. The generated structures also show similarities to natural ball lightning and can be considered a laboratory analog of this phenomenon.

Although several theoretical models of self-confined plasmoids, some of them oscillatory in nature, have been proposed in the literature i.e. [10,11,12], mostly as attempts to explain ball lightning, experimental realizations capable of producing fusion reactions have not been reported so far. Previous laboratory experiments [7,8,9] with ball-lightning-like phenomena demonstrated various interesting properties but did not observe signs of nuclear fusion.

Experimental Setup

Experiments were conducted using a custom pulsed-power generator driving a specially designed coaxial low-pressure diode. A general schematic of the device is shown in Fig. 1. Some auxiliary measurement, safety, and control systems are omitted for clarity. Fig. 2 shows a photograph of the experimental setup.

The system consists of three main subsystems: the auxiliary pulse generator, the main pulse generator,the diode assembly with vacuum and gas supply systems, and Diagnostics.

Overall Operation Principle

The device operates in a two-stage principle. The auxiliary generator first produces a low-current discharge (20–300 A) in the diode to pre-ionize the gas. When the current exceeds a preset threshold, a delayed trigger signal is sent to the main generator. The main pulse (up to 1 MV, ~5 ns duration, ~300 J) is then injected into the initial low-current discharge, causing a rapid current rise to tens of kiloamperes and the formation of a self-contained plasmoid.

Main pulse generator

Primary energy is stored in a capacitor bank 1 consisting of four series connected 50 μF, 3 kV low inductance capacitors. Discharge is initiated by a trigatron switch 4 through 24 parallel RG-58 coaxial cables into the primary winding of a Tesla transformer. The secondary winding is integrated into the first pulse forming line 5 (1 nF capacitance, 5,3 Ω, multiple layers of mylar film impregnated with glycerol). This dielectric system offers excellent dielectric strength 1 MV/cm in a practical device under microsecond pulse [13,16]. Conductors of this line are designed to be “transparent” for the magnetic field to enable the Tesla transformer to work efficiently. The transformer is capable of charging this line to 1 MV. The line has capacitive voltage sensor 6 for measuring charging voltage which can be calibrated against an external known probe. An example of charging voltage waveform can be seen on Fig. 3 (note the distortions caused by high frequency effects in a magnetically transparent shield).

The pulse is then compressed in subsequent stages:

- A seven electrode, capacitively graded transfer spark gap 7 operating at pressures up to 28 bar. Pressure is generated by air compressor, volume of gap is purged from corrosive products by vacuum pump, and valves after each discharge. This pressure system is connected to the spark gap by a copper pipe of which prepulse inductor 8 is made.
- Line 9 is a transformer oil line with an impedance of 80 Ω and 2 ns electrical length. Second pulse forming line 10 (4,2 Ω, 2,5 ns). Its dielectric is triacetin. It has dielectric constant 7.1 stable to gigahertz range and low dielectric loss [14]. Also according to our tests it has 0,64 MV dielectric strength for an effective time of 300 ns. After spark gap 7 fires, this triacetin line is charged by subsequent reflections through oil line 9 in tens of nanoseconds. It also has capacitive voltage sensor 11.
- An oil spark gap (12) separates the triacetin line 10 (4,2 Ω, 2,5 ns) from the output oil line 10 (7,5 Ω, 0,7 ns). After triacetin line charges to enough voltage, breakdown occurs and energy stored in it is switched to the diode. Gap is continuously purged with filtered oil by use of pump and filter 35. It is essential for removal of gas and carbon byproducts of discharge in oil to provide stable conditions for switching.
- A output oil line 10 (7,5 Ω, 0,7 ns) which transport pulse to the diode, and spiral oil line 17 made of 60 cm copper tubing wound on a 20 mm mandrel inside a 50 mm pipe, which reduces prepulse and simultaneously serves as the deuterium feed line to the cathode.
- A glycerol decoupling line (2,1 Ω, 2 ns) that isolates the auxiliary generator from the returning nanosecond pulse.

Auxiliary Pulse Generator

Energy is stored in a 10 μF, 12 kV capacitor 26 and switched by a high-voltage vacuum relay (DPDT contacts, Kilovac KM-14/s47). The pulse forming network 24 consists of an RL circuit, and variable 200 Ω high-power rheostat, producing a decaying pulse with a time constant of maximally 3 ms (which is typically less and it depends on particular test conditions). The discharge current is monitored by a current transformer 28, which triggers the main generator after an adjustable delay. Protection against the returning high-power

pulse is provided by an RLC filter 23 and a crowbar spark gap 22 which fires when the returning nanosecond pulse arrives, simultaneously terminating the auxiliary pulse. Auxiliary pulse is also fed to triacetin PFL through prepulse inductor 8. This ensures that electrodes of oil spark gap 12 are at the same potential. This is needed to avoid “DC” prestressing of transformer oil, because it can cause lowering of its dielectric strength in nanosecond regime [15,16] and degrade the performance of the oil switch.

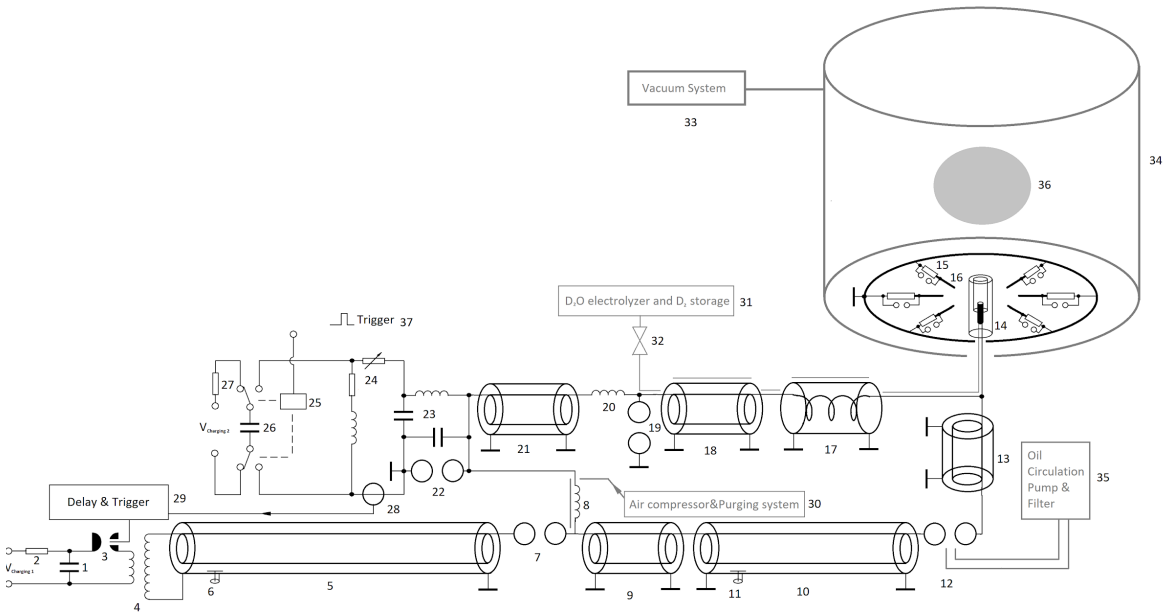

Fig. 1. Schematic of plasmoid generating device. Electrical components with grey underline are for gas transport simultaneously. 1 – main energy storage capacitor bank, 2 – charging resistor, 3 – triggered spark gap, 4 – Tesla transformer, 5 – mylar-glycerol pulse forming line, 6 – capacitive voltage sensor, 7 – pressurized spark gap, 8 – prepulse inductor/ high pressure air tube, 9 – oil line, 10 – triacetin second pulse forming line, 11 – capacitive voltage sensor, 12 – oil spark gap, 13 – oil line, 14 – cathode in dielectric sleeve, 15 – ballast resistor and commutating spark gaps network, 16 – anodes, 17 – oil spiral line/ deuterium capillary tube, 18 – glycerol line, 19 – overvoltage protection spark gap, 20 – blocking inductor, 21 – RG213 cable, 22 – protection/ crowbar spark gap, 23 – low pass filter, 24 – pulse forming circuit, 25 – vacuum relay, 26 – auxiliary energy storage capacitor, 27 – charging resistor, 28 – current transformer, 29 – delay and trigger circuitry, 30 – air compressor and purging system, 31 – heavy water electrolyser and deuterium storage, 32 – needle valve, 33 – vacuum system, 34 – glass vacuum vessel, 35 – oil circulation pump and filter, 36 – plasmoid.

Fig. 2. Photograph of the experimental setup. 1 – main energy storage capacitor bank, 2 – primary winding of Tesla transformer, 3 – mylar-glycerol line, 4 – oil line, 5 – triacetin line, 6 – oil spark gap, 7 – oil line and diode connection, 8 – vacuum chamber and diode in Faraday cage, 9 – trigatron assembly.

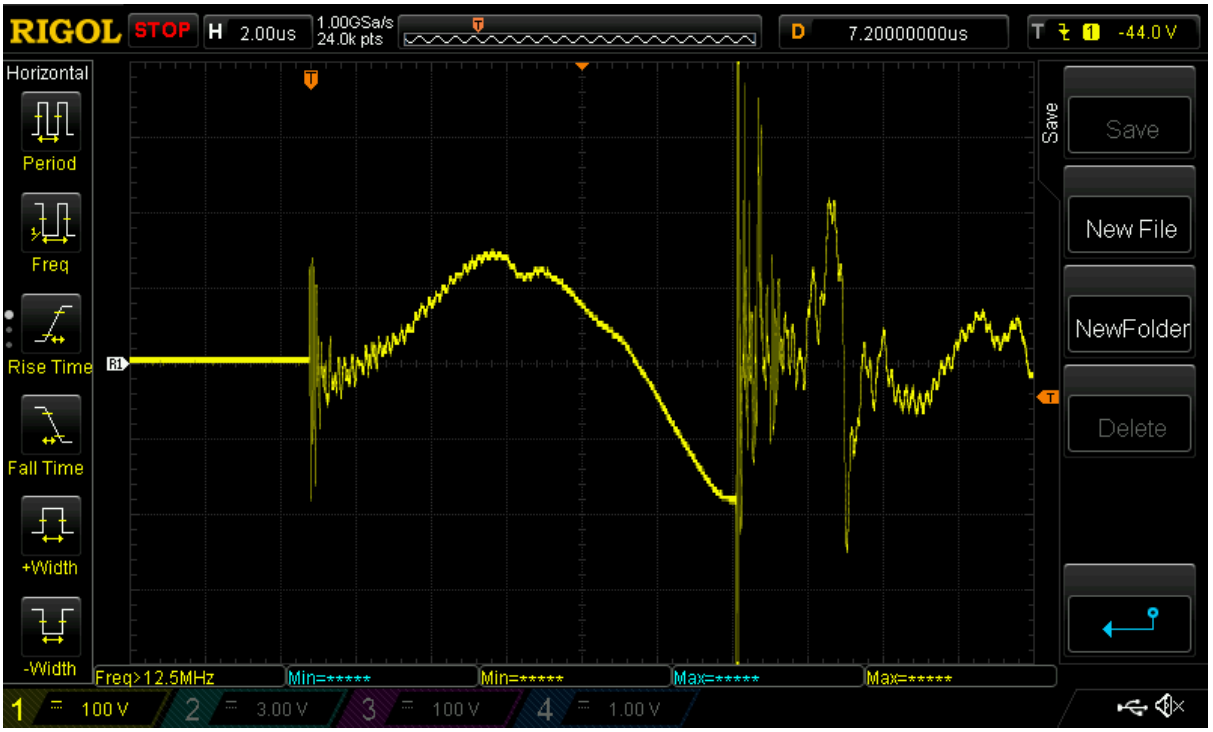

Fig. 3. Charging voltage waveform of the mylar-glycerol line. The calibration factor of the in-situ capacitive divider is 5,22 kV/V.

Diode and Vacuum System

The diode consists of a central cathode and the dielectric (i.e. epoxy) sleeve 14 surrounded by a set of concentric anodes 15. Ballast resistors connected in series with each anode ensure uniform current distribution during the phase of auxiliary discharge. In parallel with these ballast resistors, additional spark gaps are installed. These spark gaps break down due to overvoltage when the high-power nanosecond pulse arrives, and this way they reduce the impedance of the diode circuit and contribute the transition to the high-current phase.

Deuterium is injected directly into the discharge region through nozzles that are located inside the cathode. The pressure in the vacuum chamber is maintained in the range of 0,5–2 mbar using a needle valve 32 by the principle of differential pumping. The deuterium was generated by electrolysis heavy water D_2O (thermo scientific, for NMR use, 99.8% atom % D). For preparation of electrolyte, lithium metal was added to heavy water to react with it and form LiOD solution.

The vacuum vessel 34 is made of a glass pipe sealed with polycarbonate lids. The system is evacuated through a port in the upper lid. A two-stage vacuum system consisting of a rotary vane pump and a diffusion pump enables pressure control while maintaining a continuous flow of fresh deuterium through the diode.

The whole region of the diode and vacuum vessel is surrounded by a Faraday cage with detachable doors from copper mesh for observation and maintenance. It is necessary for protecting nearby electronics from electromagnetic pulse. Fig. 4 shows the view of the vacuum chamber and the diode itself.

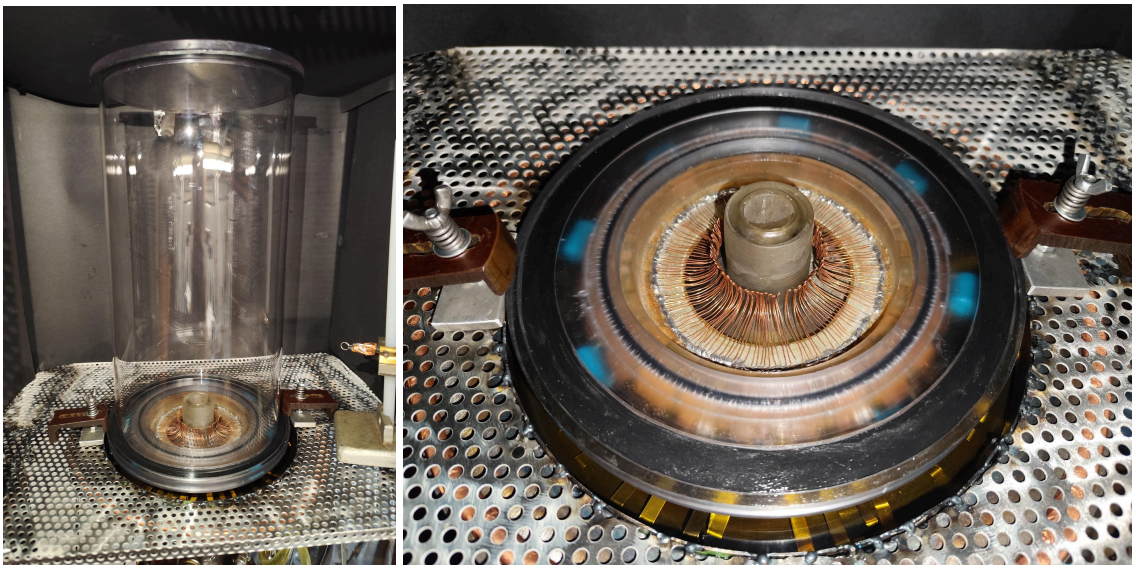

Fig. 4. Photographs of the vacuum chamber and the diode.

Electrical Diagnostics

Electrical diagnostics of the main generator are performed using two capacitive dividers 6, 11. Probes are placed in situ in mylar-glycerol line and triacetin line. Probe inside mylar line monitors charging voltage in microsecond regime. Due to high frequency effects inside the slotted shield of the line, the sensed waveform has some distortion. The probe inside the triacetin line measures its charging voltage in a nanosecond time regime. Signals from the probes are Acquisited by Digital storage oscilloscope Rigol DS1054.

Auxiliary generator has current transformer 28 for measuring current of initial discharge.

Both generators have capacitor voltage monitoring which allows control charging and safe operation of setup together with charge dump circuitry and grounding sticks.

The microwaves are sensed by a probe based on a neon tube coupled to optic fiber. The neon tube has attached a 6 mm diameter copper wire loop to its electrodes. The whole neon tube is wrapped in copper foil for screening from an external field. This screen is electrically connected to one of the neon tubes electrodes. Also there is a 1 mm hole in the screen at the tip of the neon tubes envelope for coupling to toslink optic fiber. The whole assembly is glued inside the casing of SFH551V optic fiber receiver with a removed photodiode/IC. This allows quick connection/removal of optic fiber. The optical signal is sensed by SFH250V photodiode-based receiver connected to the oscilloscope. Physical appearance of the detector can be seen on Fig. 5, and placement of it inside the Faraday cage, on Fig. 4.

The principle is as follows: the magnetic component of microwave induces a voltage on the loop. When amplitude is high enough neon ionizes, and generates light. This light is coupled to the optic fiber and transported to a photodiode receiver which produces an electrical signal from light. This signal is registered by DSO. The shield on the neon tube and magnetic pickup cause inherent high pass behaviour which ensures that the slower electromagnetic pulse from the main generator will not lit the neon tube. The threshold of detectable microwave intensity at frequency of 2,45 GHz is 540 kW/m^2.

Fig. 5. Photograph of microwave sensor.

Neutron Diagnostics

Neutron diagnostics are based on the principle of silver activation which is uses neutron capture reaction of two stable silver isotopes, ^{107}Ag and ^{109}Ag present in natural silver. Upon this reaction unstable isotopes ^{108}Ag and ^{110}Ag are produced. They undergo β-decay (with half-lives of ~24 s and ~142 s, respectively) which can be detected by means of i.e. Geiger counter. 24 s isotope is most useful for this purpose because of its higher activity.

The fast neutrons generated by fusion in the self contained plasmoid are thermalized by a 6 cm thick polyethylene moderator. Thermal neutrons activate the 0,2 mm silver sheet wound over an array of three J305 Geiger counters. Total area of silver sheet was 100 cm^2 Those counters are turned on 1 s after each shot, when all charging and power circuitry is turned off and capacitors charge is dumped which ensures that electromagnetic pulse, and X-rays, or EMI from HV circuitry will not influence the measurement. The Geiger tube counts are registered in the next 3 minutes. The counter itself is pictured on Fig. 6, placed inside the HDPE moderator on Fig. 7 and the schematic of the physical layout of the setup can be seen on Fig. 8.

As no neutron source and reference detector was available to calibrate the silver neutron counter, the sensitivity was estimated with use of the data from publication [18] about silver counters with the same working principle, by method described below.

Sensitivity of the Geiger counters 1B85 were calculated from calibration data against 1,5 mCi Co60 source [18], and was compared with sensitivity of J305 found in [19].

This was multiplied by proportion factor taking into account the amount of silver in [18] and ours, number of counters and geometry with help of [17]. The obtained sensitivity is 9,06 times less than the counter described in [18]. Uncertainty of measurement is taken as 25% and measured result of neutron yield can be considered as order of magnitude estimation. For our setup dimensions (shown in Fig. 8), and using data from [18] the estimated sensitivity of our counter is 73000 neutrons per count.

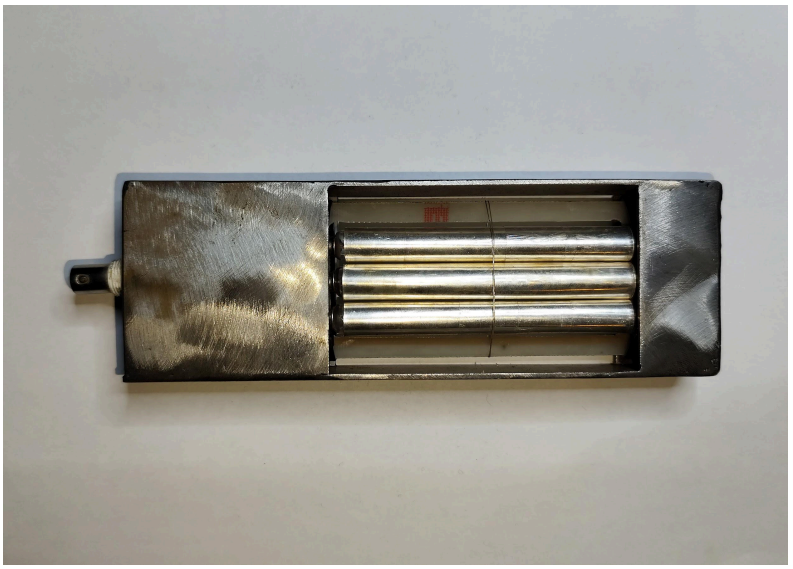

Fig. 6. Photograph of the neutron detector with an array of three J305B Geiger tubes wrapped in 0,2 mm silver sheet.

Fig. 7. Photograph of the neutron detector inside the HDPE moderator placed behind the Faraday cage.

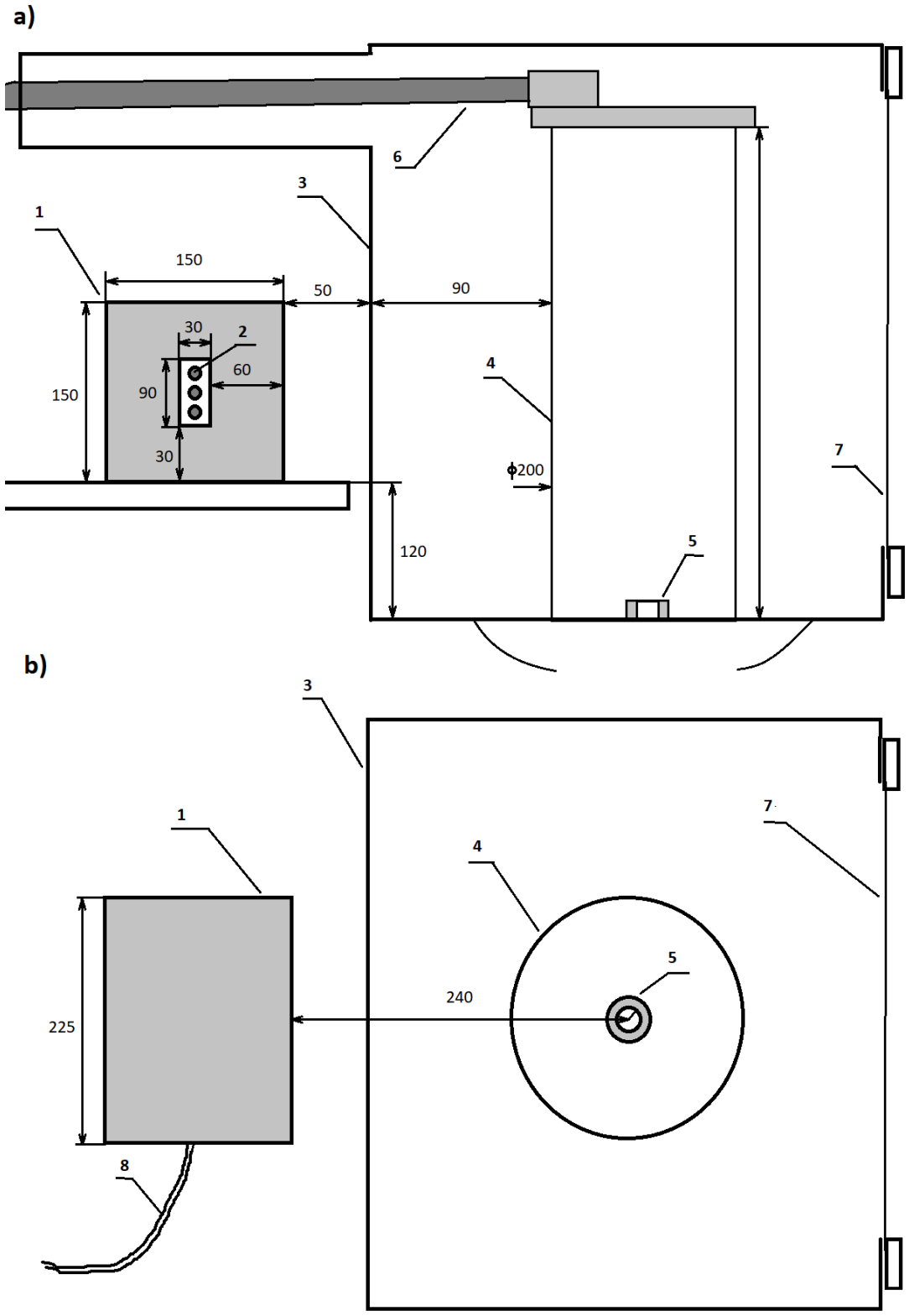

Fig. 8. Layout of the setup for neutron detection. Dimensions are in millimeters. **a)** side view **b)** top view. 1 – HDPE moderator, 2 – array of three J305 Geiger counters wrapped in 0,2 mm silver sheet, 3 – Faraday cage, 4 – vacuum chamber, 5 – diode, 6 – pipe to vacuum pumps, 7 – vacuum chamber door.

Camera

Camera is consumer grade smartphone camera operated in 240fps 720p mode. The smartphone is placed inside a Faraday cage enclosure with ITO conductive glass window for EMP protection. The camera is placed 1,4 m away from the vacuum vessel.

Proposed Theoretical Model

A useful theoretical framework for describing the long-lived plasmoids observed in this work could be provided by the force-free time-harmonic solutions to Maxwell's equations developed by Nachamkin [11]. In this model, the plasmoid consists of harmonic electromagnetic fields in which the electric and magnetic components are locally parallel

$$\mathbf{E} \times \mathbf{B} = 0,$$

resulting in a vanishing Poynting vector inside the structure. The associated fields and current are force-free, satisfying conditions

$$\nabla \times \mathbf{B} = \alpha \mathbf{B}$$

and

$$\nabla \times \mathbf{E} = -\partial \mathbf{B}/\partial t,$$

and the electromagnetic stresses are balanced by vortical motion of the plasma, leading to a self-consistent, stable entity.

We propose that when proper initial conditions are provided, the high-voltage nanosecond pulse applied to the specially designed diode is able to excite such force-free, time-harmonic electromagnetic structures.

The proposed mechanism of plasmoid formation in our diode can be divided into four main phases (which are graphically illustrated on Fig. 9).

Initial discharge

The auxiliary generator applies voltage in order of 10 kv and produces a low-current discharge (20-300 A) between the central cathode and concentric anodes. This creates an umbrella-shaped discharge.

Main pulse injection

After a controlled delay, the main high-voltage pulse (up to 1 MV, ~5 ns) is applied. The rapid voltage rise causes breakdown of the parallel spark gaps which shorts the ballast resistors and abruptly reduces the diode impedance. Electrons of the plasma channel inside dielectric sleeve are accelerated to high energies, separating from slower ions and forming a virtual

cathode. Ions gain energy by mechanism of collective acceleration, moving towards the virtual cathode.

Excitation

The virtual cathode and associated space-charge field drive coherent electron oscillations. The specific geometry of the diode and the presence of a strong tangential electric field near the end of the dielectric sleeve promote the formation of a toroidal vortex structure.

Virtual cathode moves away from the end of the dielectric sleeve, its associated space charge field starts to attract electrons towards the ion cloud at the end of the sleeve. When they are again in the region of high electric field generated by pulse they are again accelerated away from cathode and sleeves end. The tangential magnetic field at the end of the dielectric sleeve promotes the formation of toroidal vortex motion of the oscillating electrons.

Emergence of self-stable entity

When the driving pulse decays, radiative modes (non zero E × B) dissipate energy in short time after end of the pulse, leaving a non-radiative, force-free mode with much longer lifetime. Energetic ions trapped within the potential well of this oscillating electron structure can undergo D+D fusion reactions, producing neutrons.

The experimental observations suggest the resulting plasmoid can persist for dozens of milliseconds, and the radiative modes extinct in dozens to hundreds of microseconds.

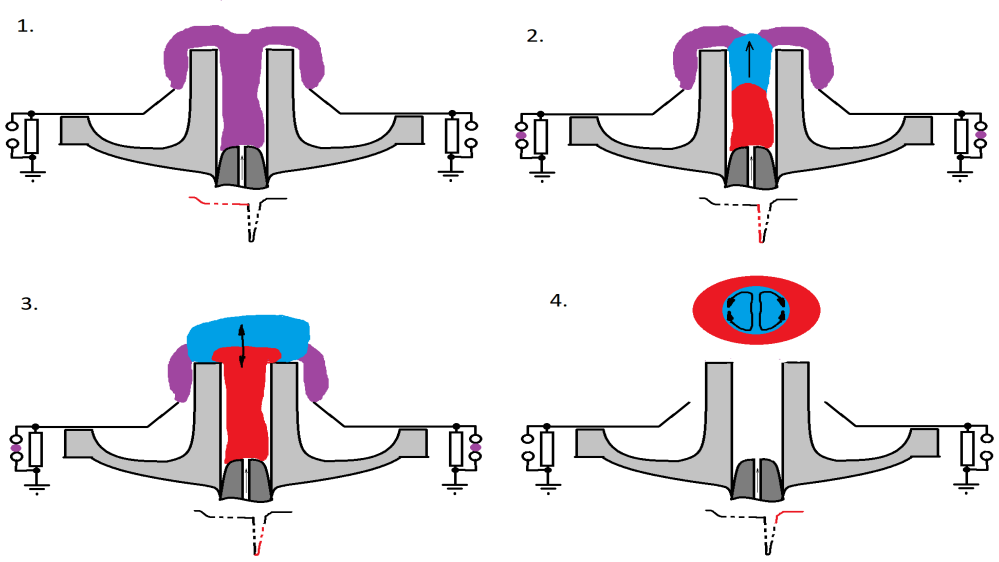

Fig. 9. Schematic illustrating the proposed concept of plasmoid formation in our diode. Black arrows show direction of motion of electrons, blue colour denotes negative space charge, red denotes positive, and violet - neutral plasma. 1. Initial discharge, 2. Main pulse injection, 3. Excitation, 4. Emergence of self-stable entity.

Results

Three types of experiments were performed. First were a series of shots on air for visual, and/or microwave observation. Second type were shots on deuterium involving a neutron counter, and third, were control shots on air with a neutron counter. Diodes with two different hole diameters in sleeve were tested: 11 mm and 22 mm. Each series of shots was performed following procedure described below (for series of first type, steps involving neutron counter were omitted)

Experimental procedure

Each shot is done in the following steps:

The deuterium is admitted to the vacuum vessel. Camera recording starts. Capacitors are charged to set voltages, and discharge initiated, generating plasmoid. During discharge electrical measurements are taken by DSO eg. microwaves, pulse waveforms. After discharge power is immediately turned off from charging power supplies and relays automatically dump capacitor energy into resistors. The silver counter is turned on. Counts are registered for the next 3 minutes. Then spark gaps 7 and 12 are purged from discharge byproducts and setup is ready for the next shot. The background radiation was measured before, and after each experimental series.

Visual observation

Each shot was recorded by a shielded consumer grade smartphone camera operated in 240fps 720p mode. Sequences of still images were extracted from recorded footage. The time interval between each frame is 4,1(6) ms. In all frames except first, there was no voltage present on electrodes of the diode, as the pulsed power system inherently immediately terminates voltage from the auxiliary generator when the main pulse is generated by use of a crowbar spark gap as described in section 2.

Parameters of each discharge registered (gas, voltage, hole diameter) are given in description of each sequence (Fig. 10 to 18). Fig. 19 shows an enlarged view of the first frame of sequence on which X-ray-caused static can be seen.

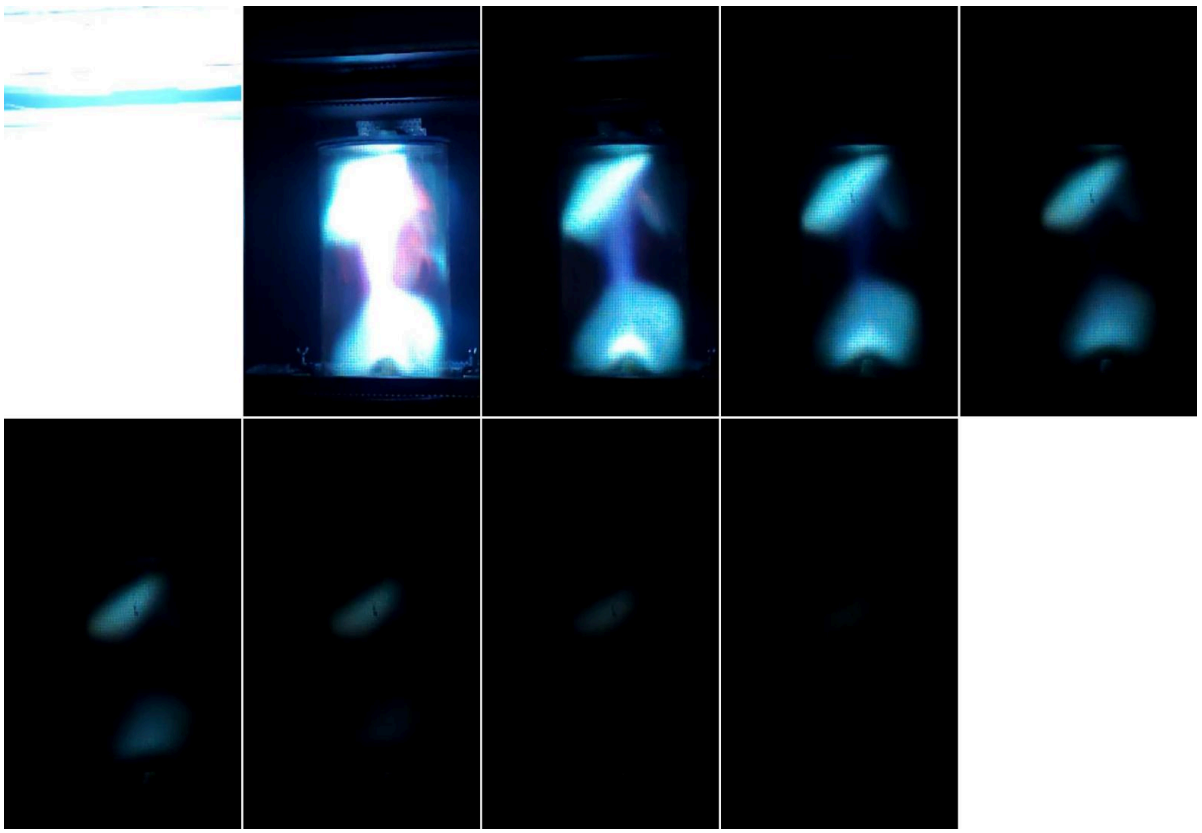

Fig. 10. Discharge on air, 2 mbar, 1 MV 1st PFL charging voltage, 11 mm hole diode.

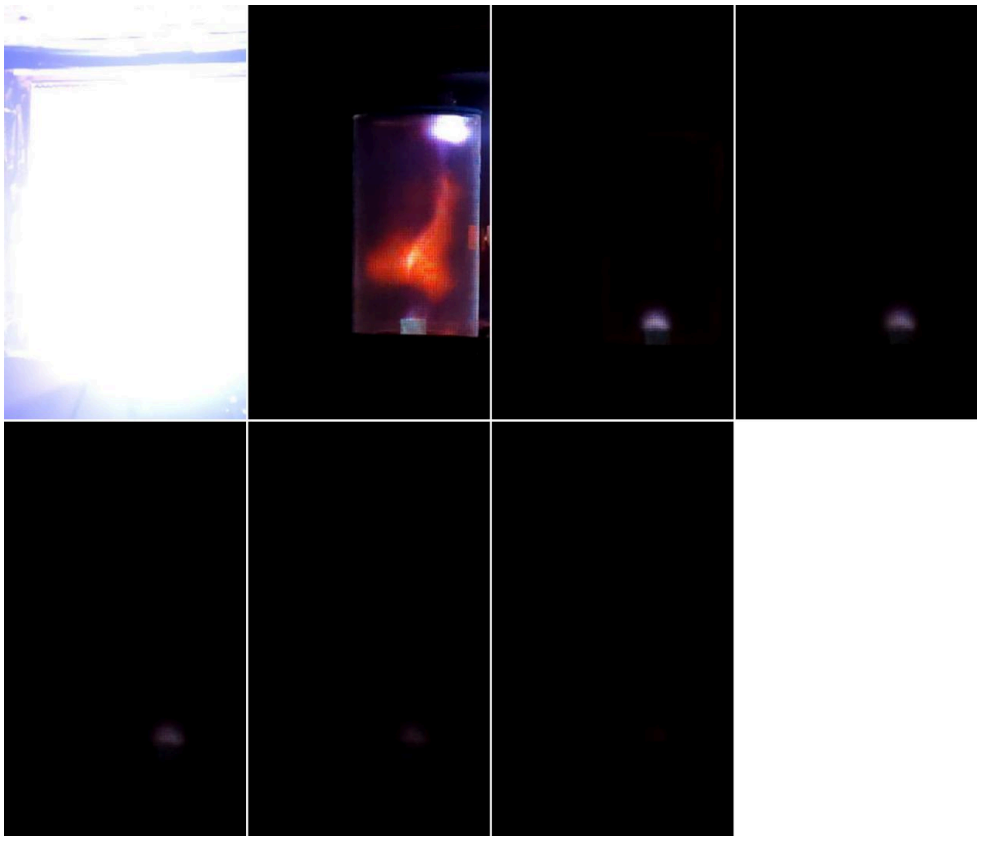

Fig. 11. Discharge on air, 2 mbar, 700 kV 1st PFL charging voltage, 22 mm hole diode.

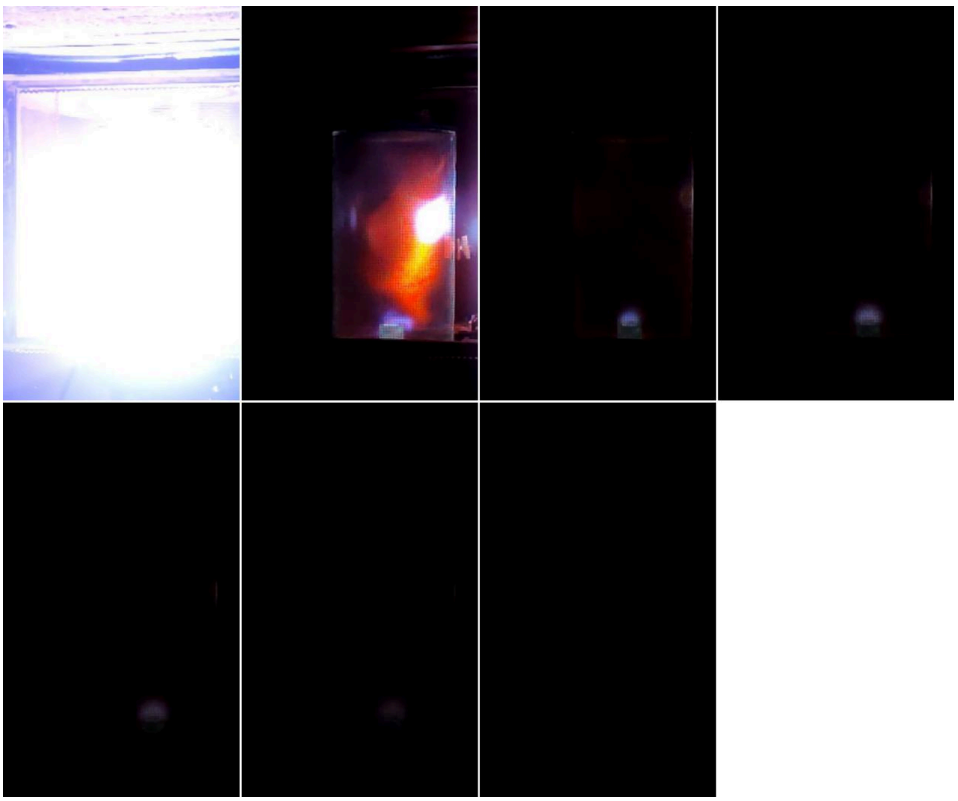

Fig. 12. Discharge on air, 2 mbar, 700 kV 1st PFL charging voltage, 22 mm hole diode.

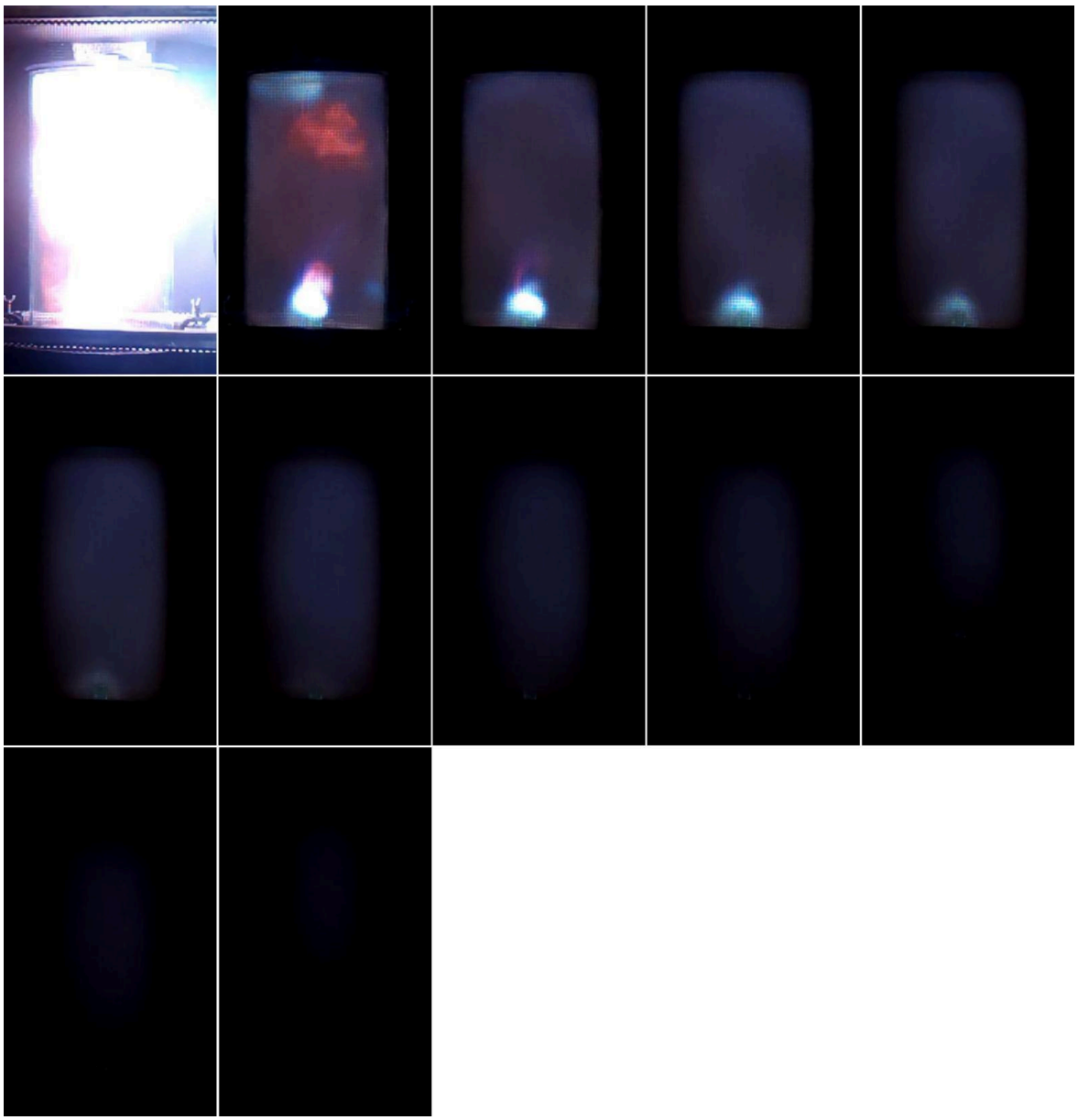

Fig. 13. Discharge on air, 1 mbar, 900 kV 1st PFL charging voltage, 11 mm hole diode.

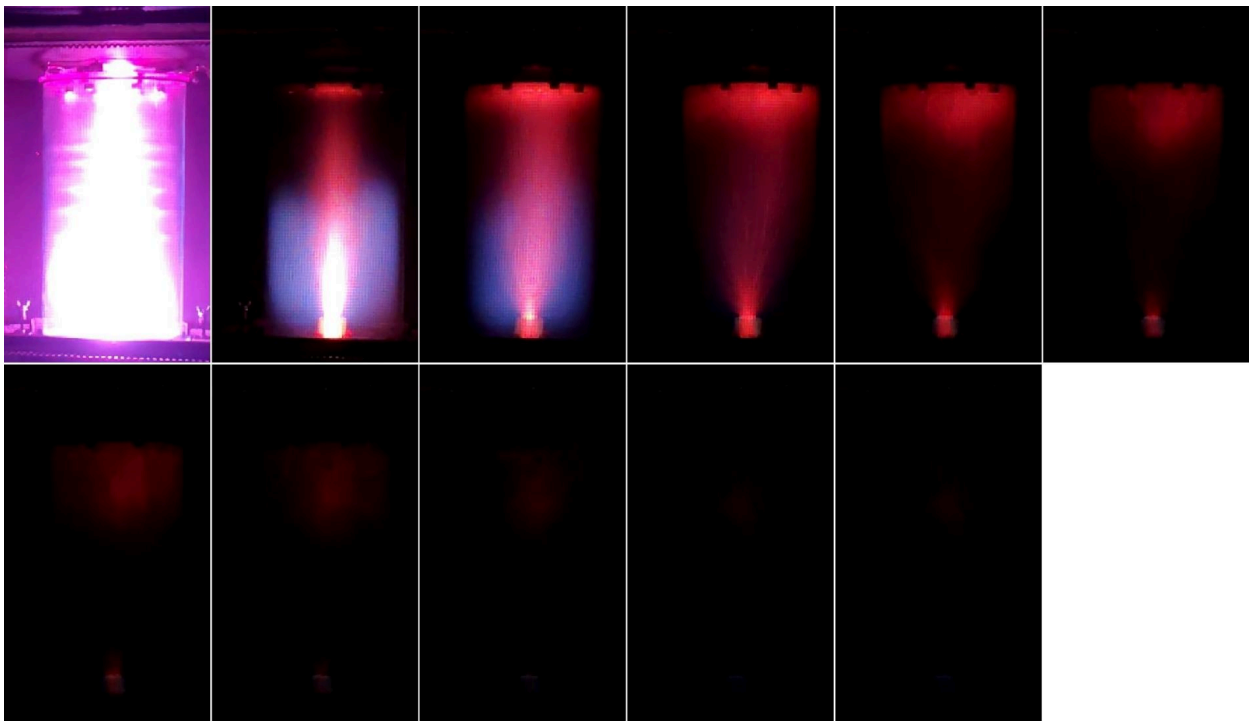

Fig. 14. Discharge on deuterium, 1 mbar, 700 kV 1st PFL charging voltage, 22 mm hole diode.

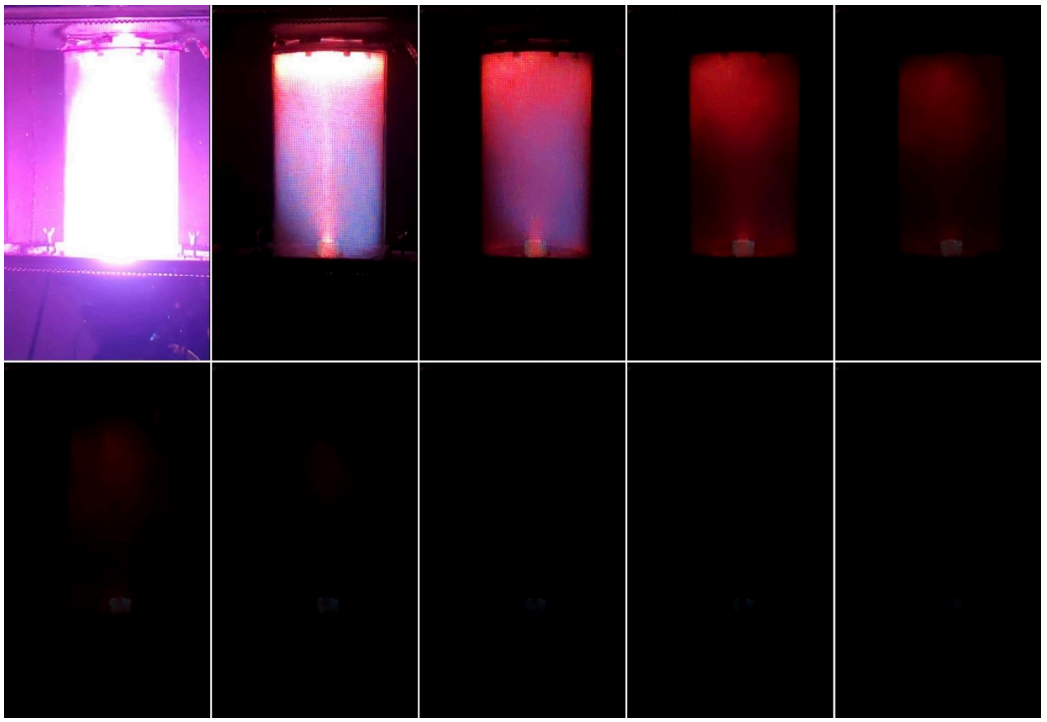

Fig. 15. Discharge on deuterium, 1 mbar, 700 kV 1st PFL charging voltage, 22 mm hole diode.

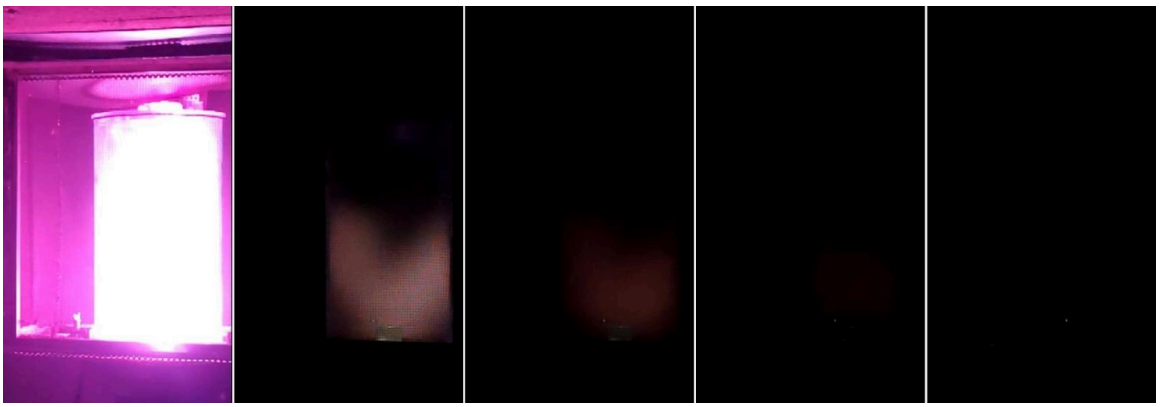

Fig. 16. Discharge on deuterium, 1 mbar, 700 kV 1st PFL charging voltage, 22 mm hole diode.

Fig. 17. Discharge on deuterium, 1 mbar, 700 kV 1st PFL charging voltage, 22 mm hole diode.

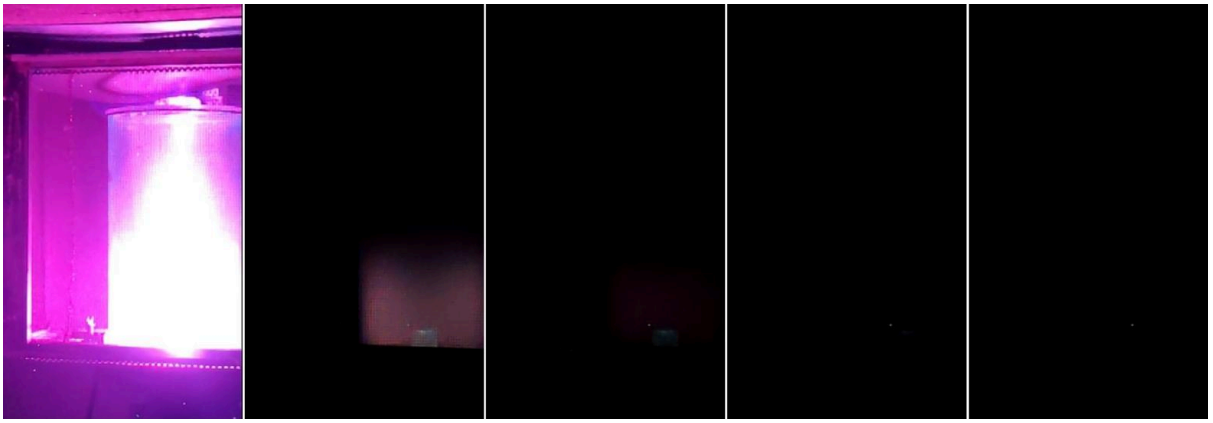

Fig. 18. Discharge on deuterium, 1 mbar, 700 kV 1st PFL charging voltage, 22 mm hole diode.

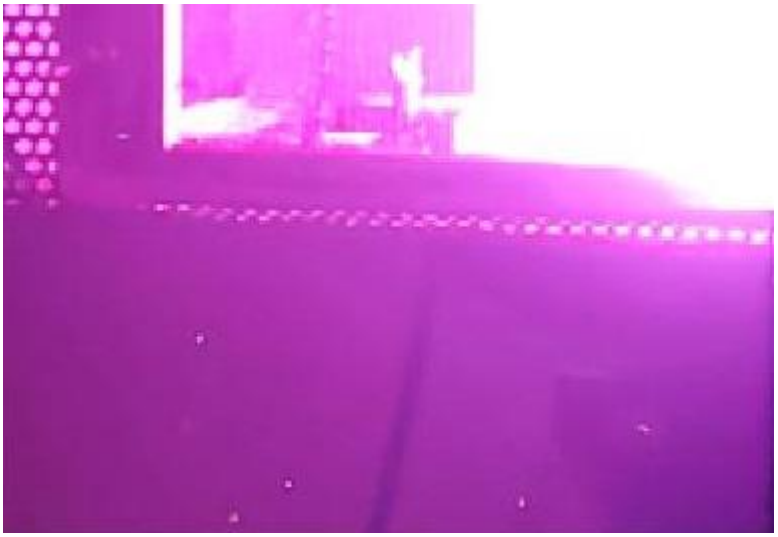

Fig. 19. Closeup on the first frame of deuterium discharge, with X-ray-caused static visible.

Microwave sensor measurements

Microwaves were measured by use of a neon tube-based microwave sensor with magnetic pickup loop, coupled optically by means of optic fiber. The signal from the photodiode receiver was recorded by DSO. Example waveforms from the receiver are shown on Fig. 20 and 21.

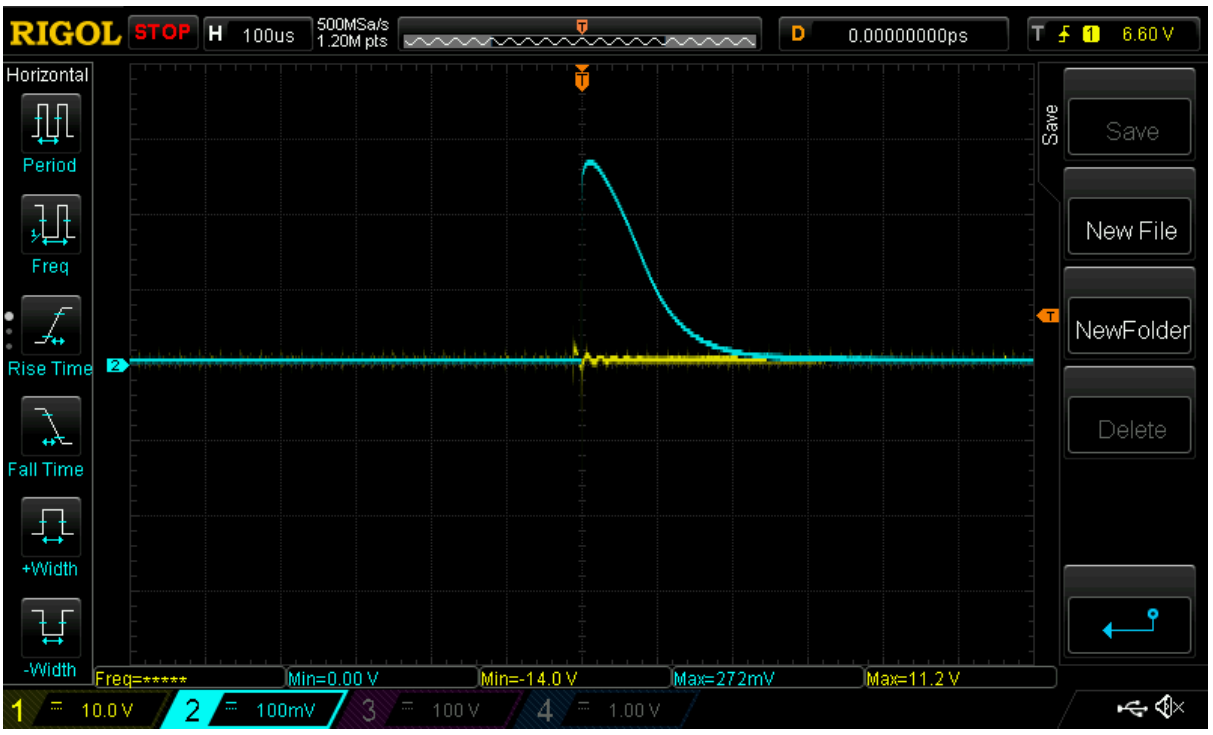

Fig. 20. Signal from microwave sensor. Charging voltage of the first PFL 800 kV. Air 1,5 mbar 22 mm hole diode.

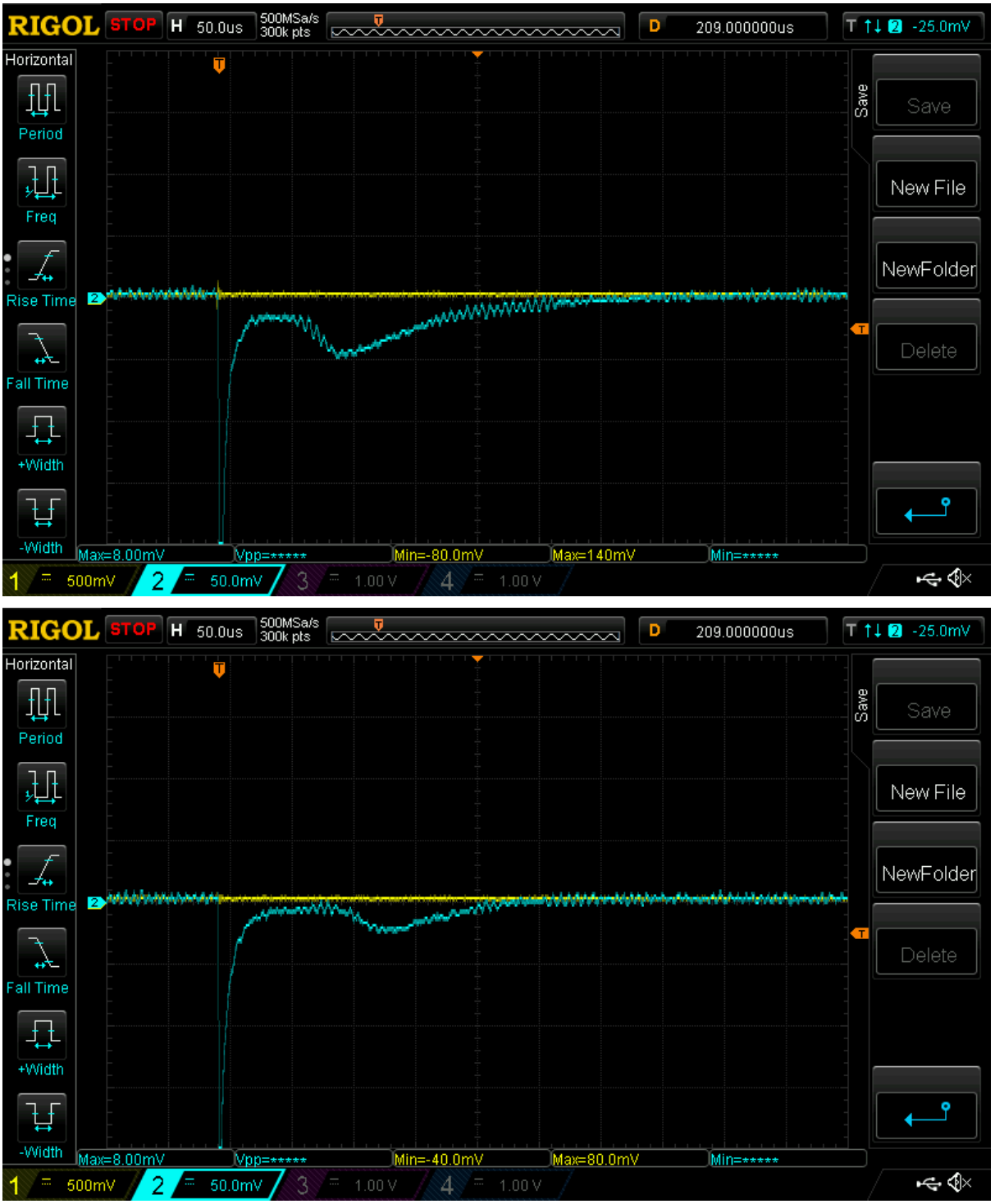

Fig. 21. Signal from microwave sensor from two different shots. Charging voltage of first PFL 400 kV. Air, 0,5 mbar. 11 mm hole diode.

The signal from 800 kV shot on air shows a ~200 μs long decay of signal. This kind of behaviour is typical for higher energy of the pulse. At lower energies decay goes faster. For example for 400 kV typical decay time around 40 μs. An unexpected behavior was observed very frequently during such lower energy shots with 11 mm hole diodes (in around ⅔ cases). The signal decays to almost zero and after tens of microseconds starts to rise and then decays.

Neutron measurements

Neutron production was studied in several series of discharges on deuterium, each consisting of tens of shots. Also control shots with similar electrical parameters with air were performed. Diodes with dielectric sleeves with two hole diameters: 11 mm and 22 mm were tested. Series with smaller diameter had a limited number of shots due to finite life of the sleeve. Dielectric breakdown typically occurs in the lower part of the sleeve ripping a 3–7 mm hole in it. Before critical failure dendrite - like carbonized traces emerged in the volume of dielectric around the place of future breakdown. When such failure occurs, long lifetime forms stop to appear. Typical life is c.a. 10 shots at 700 kV and 2–3 at 1 MV. The larger diode did not suffer any damage at 700 kV. At 1 MV it broke down after 7 shots. To achieve acceptable statistics we decided to do deuterium tests with voltage reduced to 700 kV.

Silver activation detector was used to measure the neutron yield. For each shot, radiation from the activated silver foils were counted for 3 minutes after a 1-second delay following the discharge (after pulsed power device shutdown and capacitor charge dump). Background measurements were performed before and after the series. The counts were grouped into 1 minute long intervals. The data was divided into two groups using criteria of visual lifetime. Discharges with lifetime greater than half of the longest lifetime in series were put into a group of “successful” ones, and those with lower to a “failed” group. Mean counts from each subsequent minute interval after discharge together with the previously measured background radiation level, associated p-values and pulsed power, diode and gas parameters and neutron yield are presented in Table 1 and 2. In Table 3 results of series on air are presented. Background in Table 1 and 2 is the same because two series of discharges were done one after another in the course of an hour.

	Lifetime group	Mean lifetime in group	Number of discharges	mean counts	Back-ground	Net counts	p-value	neutron yield per shot
1st min.	>25ms	45ms	15	53	45,71± 0,55	+7.23	0,0001	$5,28*10^5$
	<25ms	9ms	7	44,3		-1,41	0,62	
2nd min.	>25ms	45ms	15	45,53	45,71± 0,55	-0,28	0,92	
	<25ms	9ms	7	47,57		+1,8	0,48	
3rd min.	>25ms	45ms	15	46,47	45,71± 0,55	+0,76	0,68	
	<25ms	9ms	7	45,86		+0,15	0,96	

Table 1. Series of 22 shots on 1 mbar deuterium with 22 mm holediode, and 700 kV charging voltage.

	Lifetime group	Mean lifetime in group	Number of discharges	mean counts	Back-ground	Net counts	p-value	neutron yield per shot
1st min.	>23ms	43ms	5	57	45,71± 0,55	+9,29	0,0003	$6,78*10^5$
	<23ms	6ms	7	44,28		-1,43	0,58	
2nd min.	>23ms	43ms	5	46,6	45,71± 0,55	+0,99	0,77	
	<23ms	6ms	7	47,57		+1,8	0,48	
3rd min.	>23ms	43ms	5	47,2	45,71± 0,55	+1,49	0,63	
	<23ms	6ms	7	46		+0,29	0,92	

Table 2. Series of 12 shots on 1 mbar deuterium with 11 mm hole diode, and 700 kV charging voltage.

	Lifetime group	Mean lifetime in group	Number of discharges	mean counts	Back-ground	Net counts	p-value	neutron yield per shot
1st min.	>25ms	41ms	13	43,15	45,16± 0,7	-2,01	0,31	-
	<25ms	7ms	7	42,28		-2,88	0,27	
2nd min.	>25ms	41ms	13	43,54	45,16± 0,7	-1,62	0,41	
	<25ms	7ms	7	46,42		+1,26	0,63	
3rd min.	>25ms	41ms	13	44,77	45,16± 0,7	+0,39	0,84	
	<25ms	7ms	7	46,85		+1,69	0,52	

Table 3. Series of 12 shots on 1 mbar air with 11 mm hole diode, and 700 kV charging voltage.

It's worth mentioning that in series with a small diameter diode described here, there were two “record” discharges with number of counts greatly exceeding other "successful" ones in series. The counts are presented in Table 4. The amount of data is small, but still is statistically significant. This leads to a neutron yield of $1{,}41*10^6$ neutrons per shot.

	Mean lifetime in group	Number of discharges	mean counts	Back-ground	Net counts	p-value	neutron yield per shot
1st min.	39ms	2	65	45,71± 0,55	+19,29	0,0001	$1{,}41*10^6$
2nd min.	39ms	2	43,5	45,71± 0,55	-2,21	0,65	
3rd min.	39ms	2	49,5	45,71± 0,55	+3,79	0,43	

Table 4. Two record discharges from a series of 12 shots on 1 mbar deuterium with 11 mm hole diode, and 700 kV charging voltage.

Discussion and conclusions

The experimental results demonstrate the reproducible generation of long-lived plasmoids in a high power pulsed discharge in diode of our concept, which have observed lifetimes of tens milliseconds.

The most significant finding is the detection of silver activation consistent with D+D fusion neutron production, which appears only in deuterium discharges and is absent in control experiments performed in air under identical electrical conditions.

A clear behaviour could be concluded: measurable neutron signals emerge predominantly for plasmoids with high lifetime, which can be connected with efficiency of the energy transfer to plasmoid and its stability in specific discharge. Hence fusion seems to take place in a long lifetime entity itself after a nanosecond discharge, when no electrical power is supplied.

Typical averaged neutron yields over series recorded were for example $6{,}78*10^5$. With charging voltage 700 kV of the first PFL with capacitance of 1nF which means 245 J energy. The highest neutron yields were obtained during tests of the 11 mm diode in two record shots. The $1{,}3*10^6$ neutrons per shot was observed. Although absolute calibration of the silver activation detector was not available, the systematic difference relative to background, combined with the total number of shots (>10), and correlation with visual lifetime supports the interpretation that nuclear reactions take place inside the self-contained plasmoid structure. These results are comparable to or exceed typical neutron outputs reported for small Dense Plasma Focus devices operating in a similar energy range (100–300 J) [4,5].

Existence of “record” shots suggests there is large room for optimization, and much higher neutron generation efficiency can be achieved. Such results with a smaller diameter hole in diodes dielectric sleeve suggest higher energy density and electric fields contribute to better energy transfer. However at such electric fields dielectric material of sleeve tends to break down. Therefore finding a better material and optimizing geometry is needed. Also the role of local charge accumulation in dielectric sleeve and its mitigation should be considered.

We don't take into account energy stored in the auxiliary capacitor in discharge energy calculation, because it is used typically for 50 μs, then it is dumped by a crowbar circuit when the main pulse arrives, so only about 2% of energy is actually used; so typically 5–10 J. Efficiency could be improved by using a series mosfet/IGBT switch based modulator, but it will increase complexity, and potentially could become a source of problems, so brute force and reliable solution is now preferred.

The microwave emission measurements by use of our neon tube base optic fiber coupled detector show high power microwave emission during the first tens of microseconds after discharge. During high energy discharge the simple decay is observed in over 200 μs typically. However at lower discharge energies the emission tends to “wake up” after another tens of microseconds in a considerable number of shots. This behaviour could be consistent with our proposed theory of operation and Nachamkins model [11] for the resulting plasmoid. The microwave emission can be the effect of the formation of a virtual cathode and the long

decay observed, the radiative non force free modes of oscillation radiating out their energy. The “wake up” behavior can be caused by some sort of external destabilisation i.e. interaction with the chamber wall or with a gas stream affecting current distribution significantly and disturbing force free condition non radiative mode.

The alternative explanation could be pulse excitation of the cuboid resonant cavity. The fundamental mode of such a cavity would have approximately 0,6 GHz frequency. However, for example, the corresponding quality for decay in 200 μs (to less than threshold of neon tube sensor) could be estimated as around $2*10^5$. This value is very high as the very well made metal non-superconducting cavities could have Q in order of 10^3–10^4, and our Faraday cage is far from the ideal steel box loaded with its contents. This rules out this possibility, making the hypothesis of slow radiating away the energy from plasmoid more probable. However, the radiative mode of plasmoid also can be treated as an oscillator with the same very high quality factor, hence extremely low losses from particle collisions in plasma, which could be considered as anomalous.

The visual observation shows a typical visual lifetime of 40–50 ms. The plasmoids can have different characters. Typically its dense highly luminous formation (like on Fig. 11) or diffuse object occupying a large part of the chamber appears (like on Fig. 12). Sometimes two plasmoids can appear like those on Fig. 9. Those particular ones are connected with a kind of violet beam. Probably it's because local potential difference between surfaces of two plasmoids is present and a kind of glow discharge is produced. Another curious behaviour is that plasmoids can stay virtually motionless or move towards the diode while there is gas flow with speeds in order of 10 m/s upwards going from diode cathode to evacuation hole in the upper lid. Also the spectrum suggests that ionized gas is not pure air or deuterium in some cases. And fast gas flow does not purge them over time. It seems that plasmoid holds the ions entrapped at its birth when some contaminants like metal or organic vapour from diode components erosion could be present. Those behaviours, next to lifetime, is a property shared with ball lightning, which can ignore wind and wander freely too, and can preserve its spectrum over time. Therefore it can be considered to be a low pressure low-energy laboratory analog of ball lightning. Our mechanism of its creation hypothetically could be applicable for natural phenomena, because in atmospheric lightning even more extreme electric fields, and currents can exist, runaway electrons are present. It might be that if proper geometrical and electrical conditions exist, ball lightning could emerge from normal atmospheric lightning. The energy available is six orders or more orders of magnitude greater than in our setup, and voltage 3 orders of magnitude greater, so maybe it could enable the emergence of phenomena in atmospheric pressure with a lifetime of dozens of seconds. Also it's worth mentioning that typically on the first frame of video some “static” from X-rays passing through the camera appear, which are generated by high energy electrons hitting contents of the vacuum chamber.

The Nachamkins model together with our concept of force free structure initiation in our diode, could be useful for explaining observed results in a qualitative way. However it fails to describe both observed microwave emission together with quality factor of radiative modes, and visual lifetime, as loss of energy by collision rate of electrons with ions should end existence of the whole plasmoid within microseconds. However its long lifetime and extraordinarily high quality factor of “radiative modes” remain anomalous and need further theoretical and experimental investigation.

While the results are promising, further work is required to fully characterize phenomena and optimize the apparatus.

Future experiments will focus on:

- Calibration of the silver activation detector.
- Implementation of an additional neutron measurement method, for example scintillation detector.
- Systematic parametric study of diode geometry, gas injection conditions, diameter of dielectric sleeve with focus on smaller diameters and better dielectric material to increase both plasmoid lifetime, and neutron yield.
- Scale the device to higher energies (1–10 kJ).
- Improve high speed electrical diagnostics.
- Add spectroscopic and plasma diagnostics.
- Upgrading theoretical model.

Successful realization of these goals may lead to development of the compact efficient neutron source, and open new perspectives on fusion concepts based on electromagnetically self-contained plasmoids, and new knowledge about their anomalous behavior.

References

1. R.A., “Who 'invented' fusion?,” ITER, 01-May-2014. [Online]. Available: https://www.iter.org/mag/3/29#:~:text=Although%20the%20first%20patent%20for,fusion%20researc h%20began%20in%20earnest. [Accessed: 24-Sep-2022].

2. D. Clery, “Alternatives to tokamaks: A faster-better-cheaper route to fusion energy?,” Philos. Trans. R. Soc. A 377, 20170431 (2019).
https://doi.org/10.1098/rsta.2017.0431

3. R. W. Bussard, Method and apparatus for controlling charged particles, US Patent 4,826,646, filed 29 Oct. 1985 (issued 2 May 1989).

4. M. Krishnan, “The Dense Plasma Focus: A Versatile Dense Pinch for Diverse Applications,” IEEE Trans. Plasma Sci. 40(12), 3189–3221 (2012).
https://doi.org/10.1109/TPS.2012.2222676

5. L. Soto, “How to build a small Plasma Focus - Recipes and tricks,” ICTP School on Dense Magnetized Plasma, Trieste, Italy (2012).

6. M. Tuszewski, “Field reversed configurations,” Nucl. Fusion 28(11), 2033 (1988).
https://doi.org/10.1088/0029-5515/28/11/008

7. A. G. Oreshko and T. B. Mavlyudov, “The effect of hot plasmoid generation in high-current vortex discharge under atmospheric conditions,” IEEE Trans. Plasma Sci. 39(11), 2124–2125 (2011).
https://doi.org/10.1109/TPS.2011.2165298

8. S. E. Emelin, A. M. Astafiev, and A. L. Pirozerski, “Investigation of space-time structure of the discharge with an electrolytic anode and face-type, air half-space directed cathode (Gatchina’s discharge),” arXiv:0804.0981 [physics.plasm-ph] (2008).
https://doi.org/10.48550/arXiv.0804.0981

9. C. Seward, C. Chen, and K. Ware, “Ball lightning explained as a stable plasma toroid,” in PPPS-2001 Pulsed Power Plasma Science 2001, 28th IEEE International Conference on Plasma Science and 13th IEEE International Pulsed Power Conference, Digest of Papers (IEEE, 2001), Vol. 1, p. 201.
https://doi.org/10.1109/PPPS.2001.1002044

10. J. J. Lowke, “Birth of ball lightning,” J. Geophys. Res.: Atmos. 117(D19), D19107 (2012).
https://doi.org/10.1029/2012JD017921

11. J. Nachamkin, “Force-free time-harmonic plasmoids,” University of Dayton Research Institute Report (1992).

12. H.-C. Wu, “Relativistic-microwave theory of ball lightning,” Sci. Rep. 6, 28263 (2016).
https://doi.org/10.1038/srep28263

13. I. Smith, P. Champney, and L. Hatch, “High current pulsed electron beam generator,” in Proc. 1971 Particle Accelerator Conf. (1971), pp. 491–493.

14. J. M. Priebe, E. G. R. Taques Filho, E. L. Dall’Oglio, L. G. de Vasconcelos, L. B. Ceron, P. T. de Sousa, F. Telles, and C. A. Kuhnen, “The role of dielectric properties in the microwave glycerol acetylation and gaseous emissions of blended biodiesel,” Braz. J. Chem. Eng. 40(1), 217–236 (2023).
https://doi.org/10.1007/s43153-023-00418-8

15. I. D. Smith, “The early history of western pulsed power,” IEEE Trans. Plasma Sci. 34(5), 1585–1609 (2006).
https://doi.org/10.1109/TPS.2006.883391

16.]J. C. Martin, J. C. Martin on Pulsed Power (Advances in Pulsed Power Technology, Vol. 3) (Springer, New York, 1996).
ISBN: 0-306-45302-9

17. F. J. Mayer and H. Brysk, “Neutron detection efficiency of silver counters,” Nucl. Instrum. Methods 125(2), 323–324 (1975).
https://doi.org/10.1016/0029-554X(75)90288-8

18. R. J. Lanter and D. E. Bannerman, “Silver counter for bursts of neutrons,” Rev. Sci. Instrum. 39(10), 1588–1589 (1968).

19. IoT-devices, LLC, “Geiger tube J305: How to calculate the conversion factor of CPM to µSv/h Technical note,” (2025).
https://iot-devices.com.ua/en/geiger-tube-j305-how-to-calculate-the-conversion-factor-of-cpm-technical-note-en/